Available online at www.sciencedirect.com
SCIENCE DIRECT®
Journal of Molecular Catalysis A: Chemical 239 (2005) 249–256
JOURNAL OF MOLECULAR CATALYSIS A: CHEMICAL
www.elsevier.com/locate/molcata

Phase composition, reducibility and catalytic activity of Rh/zirconia and Rh/zirconia-ceria catalysts

J.A. Wang [a,*], T. López [b], X. Bokhimi [c], O. Novaro [c,1]

[a] *Laboratorio de Catálisis y Materiales, SEPI-ESIQIE, Instituto Politécnico Nacional, Col. Zacatenco, C. P. 07738 Mexico D.F., Mexico*
[b] *Departamento de Química, Universidad Autónoma Metropolitana-I, A. P. 55-534, 09340 México D.F., Mexico*
[c] *Instituto de Física, Universidad Nacional Autónoma de México, A. P. 20-364, 01000 México D.F., México*

Received 20 April 2005; received in revised form 9 June 2005; accepted 10 June 2005

Abstract

Phase concentrations, crystalline structures and surface or bulk reduction properties of zirconia and ceria-doped zircoina nanophases prepared via a sol–gel method were studied by X-ray diffraction (XRD) and temperature-programmed reduction (TPR) techniques. Rietveld refinement showed that both the phase composition and crystallite size of the solids depended on ceria content which related to the degree of surface and bulk reducibility. The pure zirconia and the solid doped with 1 wt% ceria consisted of tetragonal and monoclinic phases, while, the solids doped with 25 and 50 wt% ceria contained only one phase with cubic structure. Cerium incorporation into zirconia led to a crystalline structure distortion and reducibility enhancement of the resultant solids. The Rh loaded zirconia and ceria-zirconia solids would dissociate hydrogen and spillover it onto the support, lowering the temperature for both surface and bulk reduction of the support. A structural dependence of the catalytic activity for CO oxidation upon the catalysts support was observed. Catalytic activity of the Rh loaded zirconia-ceria solid solution with cubic phase is quite higher than for the catalysts with the support containing tetragonal and monoclinic phases of zirconia. The latter exhibited an inducing period in the reaction temperatures below 180 °C on the catalytic activity profile that might be a result of the relatively low reducibility of these support.

Keywords: Rhodium; Ceria-zirconia catalyst; Rietveld refinement; CO oxidation; Sol–gel synthesis

1. Introduction

Ceria and zirconia are very important catalytic materials that have been widely applied as catalyst supports, active components or promoters in many catalytic reactions [1,2]. As an example, zirconium oxide doped with iron and manganese and promoted by sulfate, is a promising catalyst for skeletal isomerization of hydrocarbons at low reaction temperature [3,4]. Zirconia has been also used in solid oxide fuel cells and oxygen sensors due to its defective structure [5,6]. One of the most important applications of ceria is as promoter in the current three-way catalysts for elimination of exhaust gases from automobiles [7,8]. The promoting effect is originally attributed to its large oxygen storage capacity and its ability of transferring lattice oxygen from bulk to surface [9,10]. It is also reported that cerium oxide may enhance metal dispersion and stabilize the support [11,12]. Although zirconium and cerium oxides play a variety of roles in many different catalytic reactions, the main drawback of these two materials is their thermal instability. For instance, the three-way catalysts usually are performed at temperatures above 500 °C, when zirconia or ceria are used as support, the catalysts may be easily deactivated at high temperature by diminishment of active surface or growth of crystallite size resulted from serious thermal sintering and phase transformation [13]. In the application of environmental catalysis, the findings to enhance thermal stability of the zirconia and ceria materials by suppressing the crystal growth are attractive subjects.

* Corresponding author. Tel.: +52 55 57206000x55124; fax: +52 55 55862728.
E-mail addresses: wang_j_a@yahoo.com, jwang@ipn.mx (J.A. Wang).
[1] Member of El Colegio Nacional de México.

1381-1169/$ – see front matter © 2005 Elsevier B.V. All rights reserved.
doi:10.1016/j.molcata.2005.06.021

In recent years, much attention has been paid to the synthesis of ceria-doped zirconia or zirconia-doped ceria materials because of their unique redox properties, enhanced oxygen storage capacity and improved thermal stability in comparison with ceria or zirconia alone [14]. A variety of synthetic methods have been applied to obtain ceria-zirconia solids for catalytic applications. These include high-temperature firing, high-energy mechanical ball-milling of ceria and zirconia mixture, coprecipitation and sol–gel techniques [15–19]. Among these methods, the sol–gel method was believed to be very beneficial to obtain nanophases of ceria-zirconia solid solution with high purity, homogeneity and well controlled properties.

In the present work, combining both zirconia and ceria components by a sol–gel synthesis approach, ceria-zirconia mixed oxides or ceria-zirconia solid solutions with nanocrystals and various phase compositions were obtained. The Rietveld method was applied to refine the crystalline structures by which the lattice cell parameters, average crystallite size and phase concentration of the solids annealed at different temperatures were quantatitively determined. The surface and bulk reducibility of the Rh_2O_3 loaded ceria-zirconia nanophases were studied by temperature-programmed reduction of hydrogen. Finally, the catalytic behaviors of the Rh loaded sol–gel ceria-zirconia catalysts for CO oxidation were evaluated.

2. Experimental

2.1. Preparation of zirconia and ceria-zirconia solids

The zirconia and zirconia-ceria mixed oxides were prepared by using zirconium-*n*-propoxide (70% $Zr(O–Bu)_4$ in propanol) and $Ce(acac)_4$ as zirconium and cerium sources. The synthesis procedure of zirconia was as follows: 11 ml of $Zr(O–Bu)_4$ were dissolved into 35.2 ml of absolute ethanol under continuous stirring to form a homogeneous solution, to which a hydrolysis catalyst (28 wt% ammonia) was dropped until reaching pH 10. Thereafter, 2 ml of water were dropped and the new solution was stirred until gelling. The gel was dried at room temperature in a vacuum for 24 h and the resultant while solid was calcined at various temperatures for 4 h in air for further characterization and structure analysis. The synthesis procedure of the zirconia-ceria mixed oxides was similar to that shown above, expect that, calculated amounts of zirconium and cerium procursors were simultaneously added to obtain a homogeneous solution. The final zirconia-ceria mixed oxides were noted as 1% CeO_2–99% ZrO_2, 25% CeO_2–75% ZrO_2 and 50% CeO_2–50% ZrO_2.

2.2. Preparation of Rh-loaded catalysts

The 0.5 wt% Rh/ZrO_2 and 0.5 wt% Rh/zirconia-ceria catalysts were prepared by impregnating the ZrO_2 and ceria-zirconia solids with the appropriated amount of $Rh(NO_3)_3$ aqueous solution. The supported metal catalysts were dried at 120 °C for 12 h and then were calcined at 600 °C for 4 h. Before the catalytic test, all the samples were reduced under 99.9% H_2 at 300 °C for 2 h.

Table 1
Atomic fractional coordinates of tetragonal zirconia (space group $P4_2/nmc$)

Atom	Site	*x*	*y*	*z*
Zr	2a	0.75	0.25	0.75
O	4d	0.25	0.25	*u*[a]

[a] 0.035 (4) < *u* < 0.048 (3).

2.3. XRD analyses and the Rietveld refinement

XRD measurements were carried out at room temperature on a Bruker D8 advance diffractometer with Cu Kα radiation and a secondary beam graphite monochromator. Intensities were obtained in the 2θ range between 20 and 110° with a step of 0.02° and a measuring time of 2.7 s for each point. Crystalline structures were refined with the Rietveld method by using FULLPROF98 code [20], which is especially designed to refine simultaneously both the structural and microstructural parameters through a least-squares method. Taking into account both the particles size and strain broadening effects, the experimental profiles were fitted with a pseudo-Voigt function. The weight fraction (W_i) for each phase was determined from the following relation:

$$W_i = \frac{S_i(NMV)_i}{\sum_j S_j(NMV)_j}\%$$

where *i* is the value of *j* for a particular phase among the *N* phases present. S_j is the corresponding refined scale factor, *N* is the number of formula units per unit cell, *M* is the atomic weight of the formula unit and the *V* is the volume of the unit cell.

For refining the crystalline structures in the different solids, the atomic fractional coordinates corresponding to tetragonal, monoclinic and cubic phases are reported in Tables 1–3, respectively. Variation limits of the atomic coordinates from low to high for the monoclinic structure in both the ZrO_2 and 1% CeO_2–99% ZrO_2 solids at 400 and 600 °C are reported in Tables 4 and 5. The standard deviations of the refinements, showing the variation of the last figures of

Table 2
Atomic coordinate of the cubic structure, space group *Fm3m* (225)

Atom	Site	*x*	*y*	*z*
Ce	4e	0.00	0.00	0.00
O	4e	0.25	0.25	0.25

Table 3
Atomic fractional coordinates of monoclinic zirconia (space group $P2_1/C$)

Atom	Site	*x*	*y*	*z*
Zr	4e	u_x	u_y	u_z
O1	4e	v_x	v_y	v_z
O2	4e	w_x	w_y	w_z

Table 4
Atomic coordinates of the monoclinic structure in the 100% zirconia

Temperature (°C)	Atom	*x*	*y*	*z*
400	Zr	0.272 (1)	0.038 (1)	0.210 (1)
	O1	0.094 (6)	0.328 (5)	0.385 (5)
	O2	0.477 (6)	0.765 (3)	0.461 (6)
600	Zr	0.2728 (7)	0.0379 (6)	0.2101 (6)
	O1	0.080 (4)	0.332 (3)	0.355 (3)
	O2	0.464 (4)	0.757 (2)	0.464 (4)

the corresponding number, are given in parentheses. When they correspond to refined parameters, their values are not estimates of the possible error in the analysis as a whole, but only of the minimum possible errors based on their normal distribution.

2.4. Measurement of temperature-programmed reduction (TPR)

The TPR experiments were performed with a Micromeritics 2900 TPD/TPR instrument that was in line with a flow system equipped with a quartz U-reactor. Prior to measurement, 100 mg of the samples were thermally treated under a dry nitrogen flow (99.99%) at 450 °C for 30 min. Afterwards, the samples were cooled down to 30 °C under the N_2 stream. In the reduction step, the sample was progressively heated from 30 to 900 °C with a heating rate of 10 °C/min. A mixture of 10% (v/v) H_2 in Ar was used as a reducing gas. The hydrogen consumption as a function of the reduction temperature was continuously monitored by a cell of thermal conductivity detector (TCD).

2.5. Catalytic evaluation

Catalytic evaluations of the catalysts for CO oxidation were carried out in a microreactor system with a catalyst loading of 100 mg. CO (8 vol% in N_2) mixed with dried air was fed into the reactor. The flow rate of CO and dried air were 20 and 40 ml/min, respectively. The effluent in the outlet of the reactor was analysed by on-line gas chromatography analysis system equipped with a thermal conductivity detector. The conversion of CO to CO_2 over the catalysts were measured at various temperatures between 50 and 400 °C. The light-off reaction temperature, T_{50}, is defined as the temperature at which the conversion of CO to CO_2 reaches 50%, while, T_{95} is the temperature at which the conversion of CO to CO_2 reaches 95%.

Table 5
Atomic coordinates of the monoclinic structure in the 1 wt% CeO_2–99 wt% ZrO_2 sample

Temperature (°C)	Atom	*x*	*y*	*z*
400	Zr	0.272 (2)	0.034 (1)	0.217 (2)
	O1	0.115 (7)	0.354 (6)	0.378 (6)
	O2	0.478 (6)	0.759 (4)	0.450 (6)
600	Zr	0.271 (1)	0.031 (1)	0.214 (6)
	O1	0.031 (6)	0.386 (5)	0.340 (3)
	O2	0.537 (4)	0.748 (2)	0.452 (4)

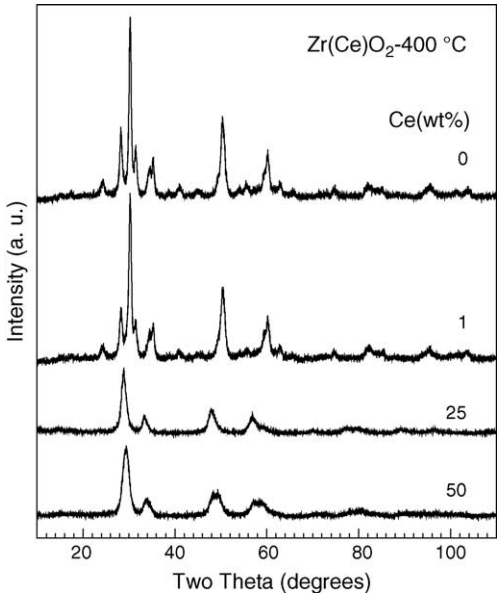

Fig. 1. XRD patterns of the samples calcined at 400 °C.

3. Results and discussion

3.1. Crystalline structure analysis and Rietveld refinement

Crystalline structures, phase compositions and lattice cell parameters of four solids were analyzed by XRD technique and refined with the Rietveld method. Figs. 1 and 2 show the

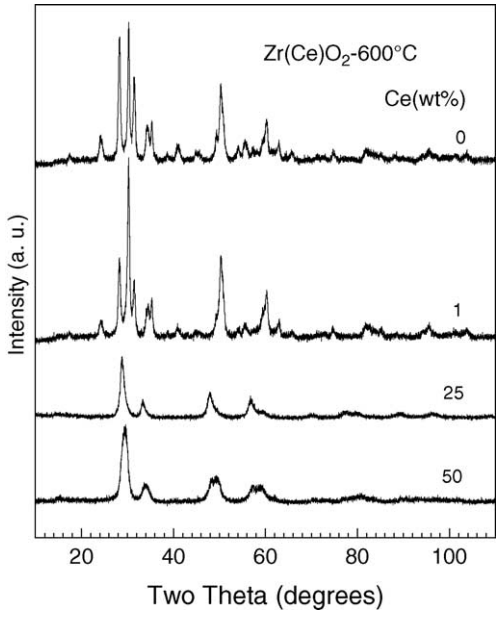

Fig. 2. XRD patterns of the samples calcined at 600 °C.

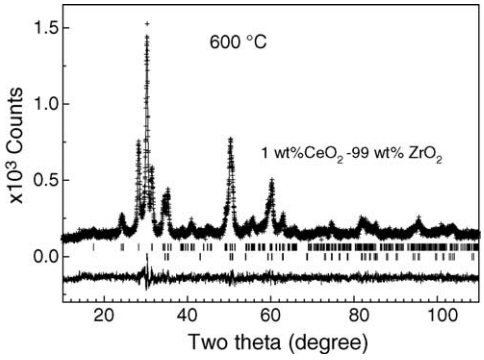

Fig. 3. A Rietveld refinement plot of the 1% CeO_2–99% ZrO_2 solid calcined at 600 °C. Experimental data are indicated by cross, and the calculated curve obtained after the refinement is indicated with a continuous line. The upper tick masks correspond to tetragonal structure and lower tick masks correspond to monoclinic structure. The continuous curve under the tick marks represents the difference between the experimental and the calculated data.

XRD patterns of the four samples calcined at 400 and 600 °C, respectively. Figs. 3 and 4 show the Rietveld refinement plots of 1% CeO_2–99% ZrO_2 and 25% CeO_2–75% ZrO_2 samples calcined at 600 °C. Phase compositions of the zirconia and ceria-zirconia samples obtained from the Rietveld refinements are reported in Table 6. The pure zirconia calcined at 400 °C consisted of 51 wt% tetraganol and 49 wt% monoclinic phase. When the sample was annealed at 600 °C, phase transformation from tetragonal to monoclinic occurred, that resulted in 17 wt% tetragonal phase further transferring to monoclinic phase. When 1 wt% ceria was incorporated into the zirconia lattice, the resultant material annealed at 400 °C chiefly consisted of 60 wt% tetragonal phase along with 40 wt% monoclinic phase, while, after 600 °C of calcination, it contained 53 wt% tetragonal and 47 wt% monoclinic, the increment of monoclinic concentration was only 7 wt% which is much less than the 17 wt% that occurred in pure zirconia. This result clearly reveals that even a very small amount of added ceria may partially inhibit zirconia phase transformation. As the ceria content increased to 25 and

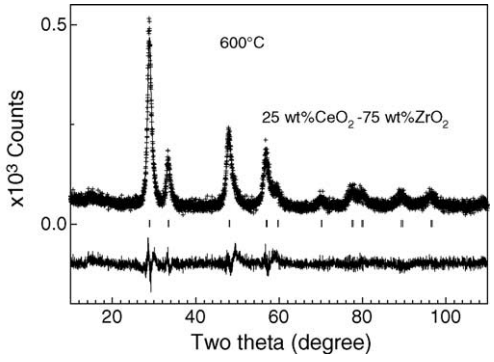

Fig. 4. A Rietveld refinement plot of the solid 25% CeO_2–75% ZrO_2 calcined at 600 °C. Experimental data are indicated by cross, and the calculated curve obtained after the refinement is indicated with a continuous line. The tick masks correspond to cubic structure. The continuous curve under the tick marks represents the difference between the experimental and the calculated data.

Table 6
Phase concentration (wt%) as a function of zirconia content

Samples	Temperature (°C)	Monoclinic	Tetragonal	Cubic
100% ZrO_2	400	49 (4)	51 (4)	
	600	67 (4)	33 (4)	
1% CeO_2–99% ZrO_2	400	40 (4)	60 (1)	
	600	47 (3)	53 (1)	
25% CeO_2–75% ZrO_2	400			100
	600			100
50% CeO_2–50% ZrO_2	400			100
	600			100

50 wt%, the samples had only one phase with cubic structure, indicating that cerium and zirconium ions are uniformly distributed forming a solid solution.

Table 7 shows the crystallite size of each phase in the different samples calcined at various temperatures. It was seen that the crystallite size linearly decreased as the cerium oxide amount increased up to 25 wt% CeO_2 at 400 °C. It diminished from 19.7 to 15.4 nm for the tetragonal phase, and 9.9 nm for the cubic phase when the cerium oxide concentration increased from 0 to 1 and 25%. When the calcination temperature was raised from 400 to 600 °C, the crystallite size of the 25% CeO_2–75% ZrO_2 sample slightly grew from 9.9 to 10.4 nm, while, that would be 15.2–22 nm for the sample containing 50 wt% ceria. These results indicate that addition of ceria into zirconia in an appropriate amount, i.e., 1 or 25 wt%, would effectively suppress phase transformations and inhibit crystal growth, and therefore, enhance the thermal stability of the solid. High concentration of ceria in the ceria-zirconia solid may result in the crystallite size larger after calcination at high temperature as in the case of 50% CeO_2–50% ZrO_2.

The lattice cell parameters of the tetragonal, monoclinic and cubic structures in the different samples annealed at 400 and 600 °C are reported in Tables 8 and 9. It is noted that the lattice cell parameter contracted 0.6% for 25% CeO_2–75%

Table 7
Average crystallite size (nm) as a function of zirconium content

Samples	Temperature (°C)	Monoclinic	Tetragonal	Cubic
100% ZrO_2	400	15.6 (5)	19.7 (5)	
	600	21.3 (6)	21.8 (6)	
1% CeO_2–99% ZrO_2	400	13.8 (6)	15.4 (1)	
	600	19.3 (8)	17.9 (4)	
25% CeO_2–75% ZrO_2	400			9.9 (2)
	600			10.4 (3)
50% CeO_2–50% ZrO_2	400			15.2 (6)
	600			22 (1)

Table 8
Lattice cell parameters (nm) as a function of zirconium content and annealing temperature

Samples	Temperature (°C)	Monoclinic				Tetragonal	
		a	*b*	*c*	*β*	*a*	*c*
100% ZrO_2	400	0.5145 (2)	0.5197 (2)	0.5312 (2)	99.02 (2)	0.3594 (1)	0.5277 (1)
	600	0.5144 (1)	0.5200 (1)	0.5314 (1)	99.06 (1)	0.3594 (1)	0.5182 (1)
1% CeO_2–99% ZrO_2	400	0.5142 (2)	0.5200 (3)	0.5311 (3)	99.96 (3)	0.3595 (1)	0.5179 (6)
	600	0.5139 (1)	0.5194 (2)	0.5312 (2)	99.01 (2)	0.3504 (1)	0.5180 (1)

Table 9
Lattice parameters (nm) as a function of zirconium content and annealing temperature

Samples	Temperature (°C)	Lattice parameter *a*	Contraction (%)[a]
25% CeO_2–75 ZrO_2	400	0.5364 (2)	0.9
	600	0.5375 (1)	0.6
50% CeO_2–50% ZrO_2	400	0.5267 (2)	2.7
	600	0.5260 (2)	2.8
CeO_2 (ref. [15])	400	0.54127 (7)	
	600	0.54095 (5)	

[a] It was calculated by comparison the lattice cell parameter *a* with that of the refereed CeO_2.

ZrO_2 and 2.8% for 50% CeO_2–50% ZrO_2, compared to pure ceria after calcination at 600 °C. The contraction of the lattice cell parameters is originated from the partial substitution of larger cerium ions by smaller zirconium ions in the structure. The contraction of the cubic lattice cell must result in a crystalline structure distortion that strongly favors the formation of defects by releasing the structural stress or microstrain induced by the contraction [9].

3.2. TPR behaviors

The surface and bulk reducibility of the four solids were studied by TPR measurement. TPR profiles are shown in Fig. 5 and the related data are reported in Table 10. For the 100% zirconia solid, no peak was observed in the TPR profile, indicating that zirconia is not an easily reducible oxide, that is in good agreement with the results of Baron et al. who reported that no noticeable hydrogen consumption was observed in TPR up to 1000 °C [21]. In the ceria-doped samples, there are two peaks in the TPR curves: one appeared at

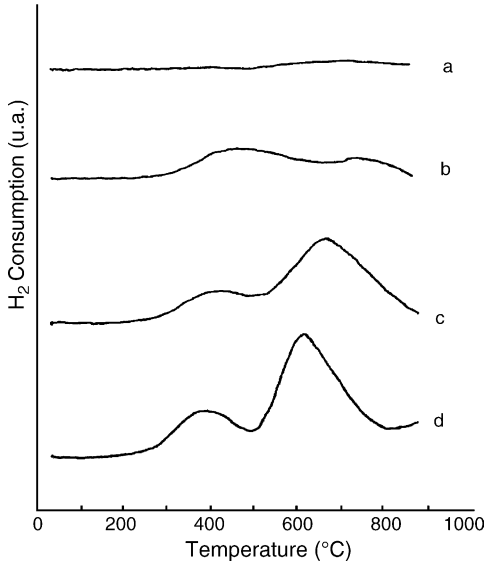

Fig. 5. TPR profiles of the solids with different cerium content. (a) 100% Rh/ZrO_2; (b) 1% CeO_2–99% ZrO_2; (c) 25% CeO_2–75% ZrO_2; (d) 50% CeO_2–50% ZrO_2.

low temperature range between 300 and 550 °C; another at high temperature range between 550 and 850 °C. The hydrogen consumption corresponding to the low temperature peak in the TPR profile could be assigned to surface reduction of the materials; while, that of the high temperature peak was attributed to the bulk redution of the solids [22]. It is found that the peak maximum at the low temperature range (T_{lm}) for the different solids almost remained the same; however, the peak maximum at the high temperature (T_{hm}) shifted towards to lower temperature range and its area (A_h) quasi linearly gained as the cerium content increased. The T_{hm} shifted 40 and 75 °C towards to low temperature range as the ceria content increased from 1 to 25 and 50 wt%. These results

Table 10
The reduction data of the support samples derived from the TPR profiles

Samples	Low temperature peak		High temperature peak		
	T_{ml}	A_l	T_{mh}	A_h	ΔT_{mh}
1% CeO_2–99% ZrO_2	450	M	720	S	
25% CeO_2–75% ZrO_2	400	M	680	L	40
50% CeO_2–50% ZrO_2	400	M	605	L	75

T_{ml}: the temperature corresponding to maximum of the peak at low temperature; T_{mh}: the temperature corresponding to maximum of the peak at high temperature; ΔT_{mh}: T_{mh} difference; $\Delta T_{mh} = T_{mh}$ (25 or 50 wt% ceria) − T_{mh} (1 wt% ceria); A_l: area of the low temperature peak; A_h: area of the high temperature peak; S: small; M: medial; L: large.

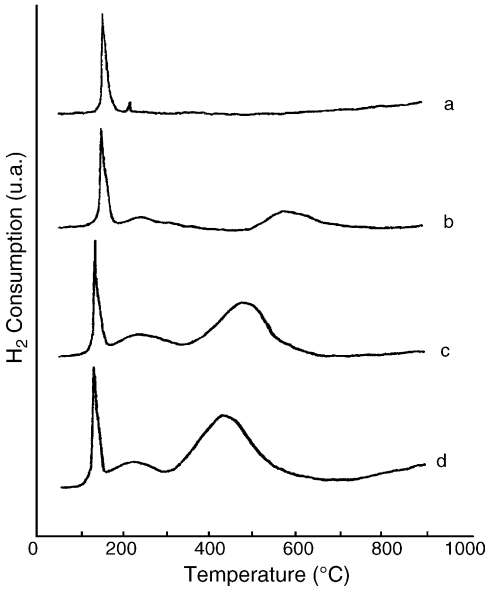

Fig. 6. TPR profiles of the $Rh_2O_3/Zr(Ce)O_2$ solids with different cerium content. (a) 100% Rh/ZrO_2; (b) 1% CeO_2–99% ZrO_2; (c) 25% CeO_2–75% ZrO_2; (d) 50% CeO_2–50% ZrO_2.

indicate that substitution of zirconium by cerium ions in the cubic structure could improve the bulk reducibility of the solids and this kind reducibility roughly increased when the cerium content in the materials increased. The reduction process proceeds in two steps, starting with the elimination of surface oxygen atoms that followed bulk reduction at higher temperature.

Fig. 6 shows the TPR profiles of Rh_2O_3/zirconia and Rh_2O_3/ceria-zirconia catalysts. In Fig. 6a, one very sharp peak and a small peak were observed around 180 and 240 °C, respectively. No other peak could be observed in the temperature above 250 °C. These two peaks were probably attributed to the reduction of the Rh_2O_3 particles. The first one is due to the reduction of the well dispersed Rh_2O_3 particles, and the small one is associated with the presence of the bulk-like crystallite in the large Rh_2O_3 particles on the surface of the support [9]. For the samples doped with ceria (Fig. 6b–d), one sharp peak below 200 °C corresponded to the reduction of the Rh_2O_3 particles as ascribed above. Differing from the sample of Rh_2O_3/ZrO_2, the small peak corresponding to the reduction of large Rh_2O_3 particles disappeared. In addition, two peaks are observed: one is between 200 and 300 °C, and the other between 300 and 600 °C. The assignments of these two peaks need to be further discussed. The peak maximized around 250 °C, as shown in Fig. 6b–d, obviously differentiates from the one at 240 °C which appeared in Fig. 6a, the former is wide with a low intensity but the latter is narrow and sharp. Therefore, the peak between 200 and 300 °C in Fig. 6b and c, is not attributed to the reduction of large Rh_2O_3 particles. It is also noted that amount of hydrogen consumption in the low temperature below 300 °C is 48.6, 101.9 and 113.4 μmol/g for the catalysts doped with 1, 25 and 50 wt% ceria, respectively; those are much more than the 7.2 μmol/g for Rh_2O_3 reduction. These results, reveal that the peaks between 200 and 300 °C in Fig. 6b–d are due to surface reduction of the support, and the peaks between 300 and 600 °C are due to bulk reduction of the support.

Compared to TPR behaviors of the bare support, both surface and bulk reduction temperatures of the Rh_2O_3 loaded samples shift to low temperatures, that is clearly related to ceria content in the support. The surface or bulk reduction of the support is also possibly affected by the reduction of Rh_2O_3 occurring during hydrogen dissociation as observed on the PdO supported $Ce_xTi_{1-x}O_2$ catalysts by Xu et al. [23]. It is reasonable to postulate that in the TPR procedure, the dispersed Rh_2O_3 particles were easily reduced by H_2 to produce metallic Rh^0 clusters. These Rh^0 clusters might adsorb H_2 and further dissociates it into H atoms, which then spillovers onto the support where both the surface and bulk oxygen is activated. As a result, the reduction of the Ce^{4+}–O ions is promoted, resulting in the TPR peak maximum corresponding to both surface and bulk reduction shifting toward lower temperature ranges, this may lead to surface reduction of the support together with rhodium oxide. These results also indicate that large Rh_2O_3 particles do not form on the surface of the ceria-doped solids, hence the Rh dispersion on these materials are high. Therefore, it can be concluded that ceria doping in the support favors improvement of Rh metal-support interaction, leading to high metal dispersion.

3.3. Catalytic activity of CO oxidation

Fig. 7 depicts the catalytic activity of the 0.5 wt% Rh/zriconia and 0.5 wt% Rh/ceria-zirconia catalysts for CO oxidation. First of all, the catalysts containing high cerium content in the support showed higher catalytic activity:

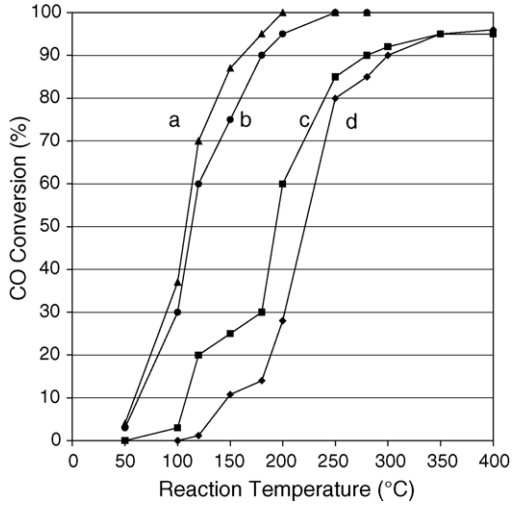

Fig. 7. CO conversion as a function of reaction temperatures over various catalysts. (a) 0.5 wt% Rh/ZrO_2; (b) 0.5 wt% Rh/1% CeO_2–99% ZrO_2; (c) 0.5 wt% Rh/1% CeO_2–99% ZrO_2; (d) 0.5 wt% Rh/1% CeO_2–99% ZrO_2.

the CO conversion over the catalysts Rh/25% CeO_2–75% ZrO_2 and Rh/50% CeO_2–50% ZrO_2 were higher than that of the Rh/1% CeO_2–99% ZrO_2 and Rh/ZrO_2. This result reveals that properties of the catalyst support have a strong impact on the catalytic activity. In the second place, the support with cubic structure was more active than that with tetraganol and monoclinic structures. The sample with cubic phase had high homogeneity in which the zirconium and cerium atoms were uniformly distributed in the lattice. In contrast, zirconia and the zirconia doped with 1 wt% ceria showed inhomogeneity in their phase composition. It is reported that the presence of different phases strongly decreases the ionic conductivity in the doped zirconia [24], which might reduce oxygen diffusion rate from bulk to surface, and is thus unfavorable to CO oxidation. Moreover, as stated above, replacement of the smaller zirconium by larger cerium ions in the cubic structure locations would lead to structural deformation and crystal microstrain, that usually result in defect formation in the structure [25]. The defective structure might facilitate oxygen ion diffusion or transfer from the bulk to the surface that also benefits CO oxidation [9].

Worth of notice in Fig. 6 is that there is an inducing period in the activity profiles for the two catalysts Rh/1% CeO_2–99% ZrO_2 and Rh/ZrO_2 under low reaction temperatures between 50 and 180 °C. The CO conversion slowly increased until the reaction temperature reached around 180 °C. The light-off temperature, T_{50}, for Rh/ZrO_2 and Rh/1% CeO_2–99% ZrO_2, was around 220 and 180 °C, respectively. However, the other two catalysts with high ceria content in the support did not show inducing behavior. The light-off temperature T_{50} for Rh/25% CeO_2–75% ZrO_2 and Rh/50% CeO_2–50% ZrO_2 was approximately 100 and 110 °C, respectively. These different catalytic behaviors are suggested to be related to redox properties of the support and interaction between the dispersed metals and the support. As shown above, pure zirconia solid has no reducibility, while, ceria exhibits excellent redox property by shifting CeO_2 under oxidizing conditions to Ce_2O_3, and the reverse under reducing condition based on the reaction $2CeO_2 \leftrightarrows Ce_2O_3 + 0.5O_2$. Ceria-doped zirconia or zirconia-doped ceria may greatly improve the reduction properties of the mixed solids [9,26,27]. The catalytic activity therefore is strongly related to cerium content, which determines the reducibility of the support. In the period of the cold start of reaction, besides the effect resulting from the dispersed metals, the surface oxygen reactivity of the support must also be taken into account because CO may react with surface oxygen to produce CO_2. Due to the high reducibility of the solids with high ceria content and cubic structure, the reactivity of surface oxygen with CO to yield CO_2 is high; thus, the initial catalytic activity of these catalysts containing high cerium content increased so rapid that no any inducing period in the low reaction temperature range is observed. However, the surface oxygen in zirconia and the 1% CeO_2–99% ZrO_2 shows low reducibility, their catalytic activity in the low reaction temperature up to 180 °C slowly increased, thus exhibited an inducing period in the low reaction temperature range. Although the reducibility of the support exhibits an important effect on the catalytic property, crystallite size, structural deformation and metal dispersion also affect the catalytic behavior. For example, the cubic structure in the 50% CeO_2–50% ZrO_2 solid shows the best reducibility as shown by the TPR experiments, however, its catalytic activity for CO oxidation is slightly lower than the catalyst doped with 25 wt% ceria, that is probably derived from the relatively larger crystallite sizes of the support (Table 7).

It was reported that rhodium ions can be incorporated into the ceria lattice upon calcination and enhance the metal dispersion and strong interaction between Rh and CeO_2 [10,28]. High metal dispersion was also assumed to be achieved by forming $Ce_{1-x}M_xO_{2-x}$ (M = Pt, Pd, etc.) [12]. High ceria content in the ceria-zirconia solid solution favors enhancement of rhodium dispersion. This might be one of the possible origins responsible for the high catalytic activity of the Rh-loaded ceria-zirconia catalysts with high ceria content.

4. Conclusion

It has been shown that crystal growth, phase concentrations and crystalline structure of the ceria-zirconia materials can be effectively controlled by incorporating cerium oxide into zirconia by the sol–gel method. The solid may consist of phases with either tetragonal and monoclinic structures or a pure cubic structure, depending on the ceria content and calcination temperature. The incorporation of cerium into zirconia greatly improves the reducibility of the solid and alters phase compositions and crystalline structures. It also enhances the thermal stability by inhibiting crystallite growth. The loaded Rh may promote the surface and bulk reduction of the support by means of hydrogen dissociation and spillover from metal to the support. The Rh/ceria-zirconia catalyst with 25 wt% ceria in the support exhibits the highest catalytic activity for CO oxidation as compared with other three catalysts, the light-off reaction temperature T_{50} is low up to 100 °C. However, over the Rh/ZrO_2 and Rh/1% CeO_2–99% ZrO_2 catalysts, CO oxidation degree shows relatively low with a short inducing period in the low reaction temperatures of 50–180 °C, that might be related to the poor reducibility of the support.

Acknowledgments

J.A. Wang would like to thank the financial support from the projects CONACyT-Mexico (Grant No. 31282-u) and FIES-IMP-IPN (Grant No. 98-29-III) and an international collaboration finding granted by CONACyT (Mexico)-NSF (China) (No. J200.489/2004). We thank Ms. Sc.M. Aguilar and A. Morales for technical support.

References

[1] A. Trovarelli, Catal. Rev. Sci. Eng. 38 (1996) 439.
[2] X. Song, A. Sayari, Catal. Rev. Sci. Eng. 38 (1996) 329.
[3] K.T. Wan, C.B. Khouw, M.E. Davis, J. Catal. 158 (1996) 311.
[4] C. Miao, W. Hua, J. Chen, Z. Gao, Catal. Lett. 37 (1996) 187.
[5] C.T. Yong, J.D. Bode, Paper No. 790143, SAE Congress, Detroit, February 1979.
[6] E.C. Subbarao (Ed.), Solid Electrolytes and Their Applications, Plenum Press, New York, 1980.
[7] A. Crucq (Ed.), Catalysis and Automotive Pollution Control II, Elseiver Science Publisher, Amsterdam/Oxford/New York/Tokyo, Stud. Surf. Sci. Catal. 71 (1991).
[8] S.H. Overbury, D.R. Huntley, D.R. Mullins, G.N. Glavee, Catal. Lett. 51 (1998) 133.
[9] P. Fornasiero, R. Di Monte, G. Ranga Rao, J. Kašpar, S. Mweriani, A. Trovarelli, M. Graziani, J. Catal. 151 (1995) 168.
[10] G.S. Zafiris, J. Girte, J. Catal. 139 (1993) 561.
[11] C. Force, J.P. Belzunegui, J. Sanz, A. Martínez-Arias, J. Soria, J. Catal. 197 (2001) 192.
[12] P. Bera, K.C. Patil, V. Jayaram, G.N. Subbanna, M.S. Hegde, J. Catal. 196 (2000) 293.
[13] M. Pijolat, M. Prin, M. Soustelle, O. Touret, J. Chem. Phys. 91 (1994) 37.
[14] E.S. Putna, T. Bunluesin, X.L. Fan, R.J. Gorte, J.M. Vohs, R.E. Lajkis, T. Egami, Catal. Today 50 (1999) 343.
[15] A. Hartridge, A.K. Bhattacharya, J. Phys. Chem. Solids 63 (2002) 441.
[16] G.W. Graham, H.W. Jen, R.W. McCabe, A.M. Straccia, L.P. Hack, Catal. Lett. 67 (2000) 99.
[17] S.H. Overbury, D.R. Huntley, D.R. Mullins, G.N. Glavee, Catal. Lett. 51 (1998) 133.
[18] A. Trovarelli, F. Zamar, J. Llorca, C. De Leitenburg, G. Dolcetti, J.T. Kiss, J. Catal. 169 (1997) 490.
[19] M. Thammachart, V. Meeyoo, T. Risksomboon, S. Osuwan, Catal. Today 68 (2001) 53.
[20] J. Rodríguez-Carbajal, Laboratoire Leon Brillouin (CEA-CNRS), France, Tel: (33) 1 6908 3343, Fax: (33) 1 6908 8261, E-mail: juan@llb.saclay.cea.fr.
[21] D.G. Barton, S.L. Soled, G.D. Meitzner, G.A. Fuenter, E. Iglesia, J. Catal. 181 (1999) 57.
[22] G. Balducci, P. Fornasiero, R. Di Monte, J. Kašpar, S. Meriani, M. Graziani, Catal. Lett. 53 (1995) 193.
[23] G. Xu, Y. Zhu, J. Ma, Y. Xie, Stud. Surf. Sci. Catal. 112 (1997) 333.
[24] K.H. Heussner, N. Claussen, J. Am. Ceram. Soc. 72 (1989) 1044.
[25] J.A. Wang, L.F. Chen, J.C. Guevara, L. Balderas-Tapia, in: S.H. Feng, J.S. Chen (Eds.), Frontiers of Solid State Chemistry, World Scientific, London/New Jersey/Tokyo/Hongkong, 2002, p. 461.
[26] F. Fajardie, J.F. Tempere, J.M. Manoli, G. Djega-Mariadassou, G. Blanchard, J. Chem. Soc. Faraday Trans. 94 (1998) 3727.
[27] G. González-Chavez, Preparation, Characterization and Catalytic Evaluation of the Catalysts Pd/$Ce_xZr_{1-x}O_2$ and Rh/$Ce_xZr_{1-x}O_2$ for NO reduction by CO, Thesis of Mater Degree, Instituto Politecnico Nacional, Mexico, 2003, p. 61.
[28] J. Soria, A. Martínez-Arias, J. Conesa, Vacuum 34 (1992) 43.